# Simulation of Stress Concentration Problems by Hexahedral Hybrid-Trefftz Finite Element Models

**F. L. S. Bussamra[1], E. Lucena Neto[1] and W. M. Ponciano[1]**

**Abstract:**   Hybrid-Trefftz stress finite elements have been applied with success to the analysis of linear and non-linear problems in structural mechanics.  Two independent fields are approximated:  stresses within the elements and displacements on their boundary.  The stress field satisfies the Trefftz constraint *a priori*, i.e., it is extracted from the Navier equation solution.  This type of element has provided remarkable improvement in stress predictions compared to the standard displacement-based finite elements. In this work, solution of stress concentration problems is carried out by hexahedral hybrid-Trefftz stress element models. Stress concentration factors and stress intensity factors are then identified and compared with available results.  The hierarchical *p*-refinement strategy is exploited in the numerical tests.

## 1   Introduction

The displacement-based finite element models are traditionally the most currently used in structural analysis because of their simplicity and general effectiveness. However, there are certain analyses in which these models are not sufficiently effective. As an example, the stress field provided by them is likely to display greater error than the displacement field. The reason for this behavior is that the stress field is obtained by differentiation of the displacement field, and differentiation discloses differences. Computed stresses are usually most accurate at locations within an element rather than on its boundaries. This is unfortunate because stresses of greatest interest usually appear at boundaries. Therefore, stresses may be calculated at certain points within an element, then extrapolated to element boundaries, or treated by some smoothing scheme. Stress smoothing is discussed by [Hinton and Campbell (1974)]; Hinton, Scott and Ricketts (1975)]. The lower quality of the predicted

---

[1] Instituto Tecnológico de Aeronáutica, 12228-900 São José dos Campos, SP, Brazil.

stress field becomes yet worse in the presence of sharp geometric discontinuities caused by cracks, holes, fillets and notches, where stresses are the most relevant mechanical quantities [Cook, Malkus, Plesha and Witt (2002); Bathe (1996)].

Mixed, hybrid and mixed-hybrid formulations have been developed to offer some advantages compared to the standard displacement-based formulation. A hybrid stress finite element formulation, for instance, is based on the independent approximation of stresses within the element and displacements on its boundary. As displacements are not favor over stresses or vice versa, a better stress description permits the improvement of the stress approximation [Kardestuncer (1988)].

Trefftz elements, a kind of hybrid elements, are known to produce accurate stress estimates. The strongest limitation in developing this type of element is the fulfillment of the Trefftz constraint, i.e., the stress bases must be extracted from the Navier equation solution of the problem being analyzed. The derivation of such bases may not be trivial. However, once these bases are secured, the advantages offered by Trefftz elements are difficult to surpass as they combine the major features of the competing finite element and boundary element methods [Freitas and Cismasiu (2001)].

Many authors have proposed the enrichment of the original approximation functions set with some novel functions. Singular solutions derived from [Williams (1952)] biharmonic stress potential are implemented to the 2-D hybrid-Trefftz elements to model high stress gradients [Freitas and Ji (1996a)] and crack problems [Freitas and Ji (1996b)]. Exploring the clouds concept to define a support region [Duarte, Babuška and Oden (2000)], the enrichment of the initial approximation stress bases is introduced in the hybrid-Trefftz formulation for plane elasticity by [Souza and Proença (2011)]. Singularities in crack problems are analyzed by Trefftz elements with collocation method by [Li, Lu and Hu (2004)].

Construction of appropriate models for heterogeneous materials may involve a formidable task due to the presence of numerous voids or inclusions and, consequently, the stress concentration around them. To deal with such issue in an attractive manner, [Dong and Atluri (2012a,b,c)] develop micromechanical models based on special Trefftz elements with built-in voids or inclusions.

[Freitas and Bussamra (2000)] have presented hybrid-Trefftz stress elements for the analysis of three-dimensional elastic problems: 6-face elements (hexahedrons) and 4-face elements (tetrahedrons). The stress bases are extracted from the Papkovitch-Neuber solution of Navier equations for isotropic material, assigning Legendre and Chebyshev polynomials to Papkovitch-Neuber potentials. These elements have shown good performance in the analysis of three-dimensional solids: no locking in the incompressibility or near incompressibility regime, low sensitivity to ele-

ment distortion (deviation from a right-angle hexahedron) and good estimates for stresses and displacements. In special, very low sensitivity to high aspect ratio (ratio between the largest and smallest element edges) was reported for the hexahedral elements in modeling thin plates. This formulation has been extended to the elastoplastic analysis of solids [Bussamra, Pimenta and Freitas (2001)] and to the analysis of laminated composite plates [Bussamra, Lucena Neto and Raimundo (2012)].

The above element attributes, in addition to the symmetry, high sparsity and well conditioning of the solving system, have motivated the use of the hexahedral elements presented by [Freitas and Bussamra (2000)] to handle thin plates with geometric discontinuities. Solution of stress concentration problems is carried out and comparison of the obtained stress concentration factors and stress intensity factors is made with available results. The hierarchical *p*-refinement strategy is exploited in the numerical tests. It is shown that good results can be directly computed with relatively coarse meshes.

## 2 Finite element formulation

Let V be the domain of a typical finite element and $\Gamma$ its boundary. Let $\Gamma_u$ and $\Gamma_\sigma$ be the portions of $\Gamma$ on which displacements and tractions are specified, respectively. The equilibrium equations and strain-displacement relations are

$$\mathbf{D}\boldsymbol{\sigma} = \mathbf{0} \quad \text{in} \quad V \qquad \boldsymbol{\varepsilon} = \mathbf{D}^\mathrm{T}\mathbf{u} \quad \text{in} \quad V, \tag{1}$$

where $\mathbf{u}$ is the displacement vector, $\boldsymbol{\sigma}$ and $\boldsymbol{\varepsilon}$ are vectors which collect the independent components of stress and strain tensors and $\mathbf{D}$ is a differential operator. Body forces and residual stress are not taken into account for simplicity. On the boundary,

$$\mathbf{N}\boldsymbol{\sigma} = \mathbf{t}_\Gamma \quad \text{on} \quad \Gamma_\sigma \qquad \mathbf{u} = \mathbf{u}_\Gamma \quad \text{on} \quad \Gamma_u. \tag{2}$$

Matrix $\mathbf{N}$ contains the components of the unit outward normal vector to $\Gamma$; vectors $\mathbf{t}_\Gamma$ and $\mathbf{u}_\Gamma$ are the specified surface tractions on $\Gamma_\sigma$ and displacements on $\Gamma_u$. The stress-strain relations of a linearly hyperelastic material are denoted by

$$\boldsymbol{\sigma} = \mathbf{k}\boldsymbol{\varepsilon} \quad \text{in} V, \tag{3}$$

where $\mathbf{k}$ is the $6 \times 6$ material stiffness matrix.

### 2.1 Approximations

The Hybrid-Trefftz elements are based on the direct and independent approximations of stress $\boldsymbol{\sigma}$ in V and displacement $\tilde{\mathbf{u}}$ on $\Gamma_\sigma$ and also on the interelement bound-

ary $\Gamma_i$ ($\Gamma_u \cup \Gamma_\sigma \cup \Gamma_i = \Gamma$; $\Gamma_u \cap \Gamma_\sigma \cap \Gamma_i = \emptyset$):

$$\boldsymbol{\sigma} = \mathbf{SX} \quad \text{in} \quad V \qquad\qquad \mathbf{\tilde{u}} = \mathbf{Zq} \quad \text{on} \quad \Gamma_\sigma, \Gamma_i \qquad\qquad (4)$$

Matrices $\mathbf{S}$ and $\mathbf{Z}$ collect the approximation functions and vectors $\mathbf{X}$ and $\mathbf{q}$ collect the corresponding weights.

The equilibrium equations can be expressed in terms of the displacement field by

$$\mathbf{DkD}^{\mathrm{T}}\mathbf{u} = \mathbf{0} \quad \text{in} \quad V, \qquad\qquad (5)$$

known as Navier equations. Trefftz constraint requires a choice of $\mathbf{S}$ such that $\mathbf{u}$ within the element satisfies (5). The stress is then determined from the displacement by means of

$$\boldsymbol{\sigma} = \mathbf{kD}^{\mathrm{T}}\mathbf{u} \quad \text{in} \quad V. \qquad\qquad (6)$$

If the displacement is written as

$$\mathbf{u} = \mathbf{UX} + \mathbf{u}_r \quad \text{in} \quad V, \qquad\qquad (7)$$

where $\mathbf{u}_r$ collects the rigid-body displacement components and $\mathbf{U}$ collects functions related to the displacement basis, one gets from (4) and (6)

$$\mathbf{S} = \mathbf{kD}^{\mathrm{T}}\mathbf{U} \quad \text{in} \quad V. \qquad\qquad (8)$$

## 2.2   On the choice of U

Each column of $\mathbf{U}$ is stated as a Papkovitch-Neuber solution of (5) for isotropic material:

$$-4(1-\nu)\boldsymbol{\psi} + \nabla(\mathbf{r}^{\mathrm{T}}\boldsymbol{\psi} + \phi) \qquad\qquad (9)$$

where $\boldsymbol{\psi}$ and $\phi$ are vector and scalar harmonic displacement potentials, respectively, $\mathbf{r}$ the position vector, $\nabla$ the gradient operator and $\nu$ the Poisson's ratio [Slaughter (2002)].

Legendre and Chebychev polynomials are attributed to $\boldsymbol{\psi}$ and $\phi$, as explained in [Freitas and Bussamra (2000)], in order to generate a displacement basis $\mathbf{U}$. Linearly dependent modes, *i.e.*, linearly dependent columns of $\mathbf{U}$, eventually introduced in this process are eliminated. The stress basis (8) is then described by 186 complete, linearly independent polynomial modes of degree $d_\sigma = 6$. Higher degrees are possible, but incomplete bases are generated. For degrees 7, 8 and 9, for instance, the stress bases have 231, 278 and 326 independent modes with deficits of 6, 16 and 31 modes to be completed, respectively.

A complete polynomial basis of degree $d_\sigma \leq 6$ is explicitly written in the computer code. In this case, linearly dependent modes generated by Legendre and Chebyshev associated polynomials have been detected and eliminated *a priori* from the stress basis **S**. For greater polynomial degrees $d_\sigma > 6$, polynomials are recursively calculated so that linearly dependent modes detection and elimination are performed during the solving system solution, when a zero, or an almost zero, pivot is found in the Gauss elimination process. Construction of complete and linearly independent sets of Papkovich-Neuber solutions in polynomial form can be found in [Fu, Yuan, Cen and Tian (2012); Wang, Xu and Zhao (2012)].

### 2.3   On the choice of Z

Displacements on $\Gamma_\sigma$ and $\Gamma_i$ are approximated by independent hierarchical monomial bases, following the Pascal's triangle scheme in a local coordinate system $(\zeta_1, \zeta_2)$ with $-1 \leq \zeta_i \leq 1$, assigned to each one of the 6 faces of the master cubic element [Cook, Malkus, Plesha and Witt (2002)]. As there are three displacement components, the number of independent displacement modes on each face is

$$n_f = \frac{3}{2}(n+1)(n+2) \tag{10}$$

for a polynomial of degree *n*.

### 2.4   Element matrices

The element is based on the variational expressions

$$\int_\Gamma (\mathbf{N}\delta\boldsymbol{\sigma})^{\mathrm{T}}\mathbf{u}\mathrm{d}\Gamma - \int_{\Gamma_\sigma \cup \Gamma_i} (\mathbf{N}\delta\boldsymbol{\sigma})^{T} \tilde{\mathbf{u}}\mathrm{d}\Gamma - \int_{\Gamma_u} (\mathbf{N}\delta\boldsymbol{\sigma})^{\mathrm{T}}\mathbf{u}_\Gamma \mathrm{d}\Gamma = 0$$

$$\int_{\Gamma_\sigma \cup \Gamma_i} \delta\tilde{\mathbf{u}}^{\mathrm{T}}\mathbf{N}\boldsymbol{\sigma}\mathrm{d}\Gamma - \int_{\Gamma_\sigma} \delta\tilde{\mathbf{u}}^{\mathrm{T}}\mathbf{t}_\Gamma \mathrm{d}\Gamma = 0, \tag{11}$$

which require that the approximation of the stress field $\boldsymbol{\sigma}$ must be extracted from the Navier equation solution and the approximation of the displacement field $\tilde{\mathbf{u}}$ must be the same along the common boundaries of any two adjacent elements [Washizu (1982); Fung and Tong (2001); Wunderlich and Pilkey (2002)]. There is no other constraint to be satisfied.

The divergence theorem allows to write

$$\int_V \delta\boldsymbol{\sigma}^{\mathrm{T}} \left(\mathbf{D}^{\mathrm{T}}\mathbf{u}_{\mathrm{r}}\right)\mathrm{dV} = \int_\Gamma (\mathbf{N}\,\delta\boldsymbol{\sigma})^{\mathrm{T}}\mathbf{u}_{\mathrm{r}}\mathrm{d}\Gamma - \int_V (\mathbf{D}\,\delta\boldsymbol{\sigma})^{\mathrm{T}}\mathbf{u}_{\mathrm{r}}\mathrm{dV}, \tag{12}$$

which reduces to

$$\int_\Gamma (\mathbf{N}\delta\boldsymbol{\sigma})^\mathrm{T}\mathbf{u}_\mathrm{r}d\Gamma = 0 \tag{13}$$

since $\mathbf{D}^\mathrm{T}\mathbf{u}_\mathrm{r}$ and $\mathbf{D}\delta\boldsymbol{\sigma}$ are both null vectors. In view of (13), substitution of the approximations (4) and (7) into (11) yields the discrete equations

$$\mathbf{F}\mathbf{X} - \mathbf{A}\mathbf{q} = \mathbf{v}$$

$$\mathbf{A}^\mathrm{T}\mathbf{X} = \mathbf{Q} \tag{14}$$

or

$$\begin{bmatrix} \mathbf{F} & -\mathbf{A} \\ -\mathbf{A}^\mathrm{T} & 0 \end{bmatrix} \left\{ \begin{array}{c} \mathbf{X} \\ \mathbf{q} \end{array} \right\} = \left\{ \begin{array}{c} \mathbf{v} \\ -\mathbf{Q} \end{array} \right\}, \tag{15}$$

where

$$\mathbf{F} = \int_\Gamma (\mathbf{N}\mathbf{S})^\mathrm{T}\mathbf{U}d\Gamma \qquad \mathbf{A} = \int_{\Gamma_\sigma \cup \Gamma_i} (\mathbf{N}\mathbf{S})^\mathrm{T}\mathbf{Z}d\Gamma$$

$$\mathbf{v} = \int_{\Gamma_u} (\mathbf{N}\mathbf{S})^\mathrm{T}\mathbf{u}_\Gamma d\Gamma \qquad \mathbf{Q} = \int_{\Gamma_\sigma} \mathbf{Z}^\mathrm{T}\mathbf{t}_\Gamma d\Gamma. \tag{16}$$

All integrals in (16) are exactly integrated by Gauss-Legendre quadrature with the minimum number of points required.

As $\boldsymbol{\sigma}$ is chosen independently for each element, $\mathbf{X}$ can be eliminated from the element equation (15),

$$\mathbf{X} = \mathbf{F}^{-1}(\mathbf{v} + \mathbf{A}\mathbf{q}), \tag{17}$$

by assuming that the matrix $\mathbf{F}$ is nonsingular, to give

$$\mathbf{A}^\mathrm{T}\mathbf{F}^{-1}\mathbf{A}\mathbf{q} = \mathbf{Q} - \mathbf{A}^\mathrm{T}\mathbf{F}^{-1}\mathbf{v}. \tag{18}$$

Let $n_X$ and $n_q$ be the number of stress and displacement parameters in $\mathbf{X}$ and $\mathbf{q}$. Then

$$\text{rank of} \quad \mathbf{A}^\mathrm{T}\mathbf{F}^{-1}\mathbf{A} \le \min(n_X, n_q - 6) \tag{19}$$

where 6 is the number of rigid body modes associated with the basis $\mathbf{Z}$. The rank of the matrix will be deficient and there will be spurious modes if $n_X < n_q - 6$ [Fung

and Tong (2001)]. In accordance with [Pian (1995); Pian and Wu (2006)], suppression of spurious modes, as it is done in this paper whenever a linearly dependent mode is detected, is the practical procedure for satisfying the mathematical form of a stability criterion, namely the LBB condition [Babuška (1973); Brezzi (1974)]. The restriction $n_X < n_q - 6$ for an individual element is necessary, but not sufficient, to ensure the satisfaction of the LBB condition.

A hybrid element becomes stiffer as the number $n_X$ increases, and usually becomes more flexible as the number $n_q$ increases. One cannot say in general that a model built of hybrid elements will be either stiffer or more flexible than the mathematically exact solution. The optimal relation between $n_X$ and $n_q$ should be found by numerical experimentation.

Some comments are in order on the numerical solution of the assembled set of equations of a finite element model. Because the assembled square matrix is symmetric and highly sparse, substantial memory is saved by storing only its nonzero entries, located in the upper triangle, in a three-column matrix with each row containing a nonzero entry and its position (row and column) in the original square matrix. Sparsity, defined as the ratio between the number of zero elements of the square matrix and its total number of elements, is typically greater than 99%. Symbolic Cholesky decomposition is applied to reduce fill-in, and then direct Gauss elimination method is applied to find the solution [Pissanetsky (1984)].

To increase the sparsity and also improve the conditioning a little more, the origin of the local Cartesian coordinate system is positioned at each element centroid. Material properties and geometric dimensions are scaled properly and advantage has been taken of the fact that identical elements, wherever are placed, have the same submatrix **F**.

## 3   Numerical tests

Three examples have been chosen to illustrate the performance of the hybrid-Trefftz formulation in the analysis of stress concentration in plates subjected to a uniformly distributed edge load $q$. All the examples are three-dimensional models of isotropic rectangular plates with thickness $h$, length $L$, width $H$, Young's modulus $E$ and Poisson's ratio $\nu$. The relevant data for the numerical analysis are summarized in Tab. 1 (consistent units are used). Although just one layer of elements is adopted in the thickness direction, the discretization can still be improved under $p$-refinement in that direction.

Neither the formulation nor the approximation bases constrain the element geometry, which may be non-convex or multiple connected. However, and for simplicity, only one cubic master element is employed.

Table 1: Data for the numerical analysis

| Example | $q$ | $E$ | $v$ | $L$ | $H$ | $h$ |
|---------|-----|-----|-----|-----|-----|-----|
| 3.1 | 1 | 1 | 0.2 | 150 | 50 | 5 |
| 3.2 | 1 | 1 | 0.3 | 30 | 10 | 1 |
| 3.3 | 10 | 1 | 0.3 | 30 | 10 | 1 |

Several hybrid-Trefftz stress elements, identified by HTS($d_\sigma$,$d_u$), are tested. The symbol $d_u$ stands for the degree adopted for displacement polynomial approximation in each element face and $d_\sigma$, as already defined, is the degree of the stress polynomial approximation. Elements with $d_\sigma > 6$ will involve incomplete stress basis.

### 3.1   Notched plate

The first set of tests is concerned with stress concentration factor calculation in a double notched plate, as depicted in Fig. 1. The plate has half-circular notches with radius $r$, the left edge fixed and the right one submitted to the action of a uniformly distributed load $q$, and refers to a Cartesian coordinate system with the $xy$-plane located in the plate midsurface.
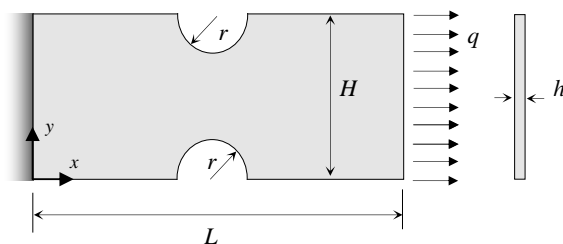


Figure 1: Notched plate.

Figure 2 shows the meshes used in the notched plate analysis, with 38, 36 and 52 elements. The convergence of the stress concentration factor $K_t$ is verified with different degrees of polynomial stress approximation $d_\sigma$ in the element domain and displacements $d_u$ in the element boundary. The stress concentration factor is defined as the ratio between the maximum stress $\sigma_{xx}$, evaluated in the plate midsurface at $(x,y) = (L/2, r)$ or $(L/2, H-r)$, and the nominal stress $\sigma_n = qH/(H-2r)$.
Figure 3 summarizes the results for $K_t/K_{tn}$ obtained with $r = 0.4\,H$, where the

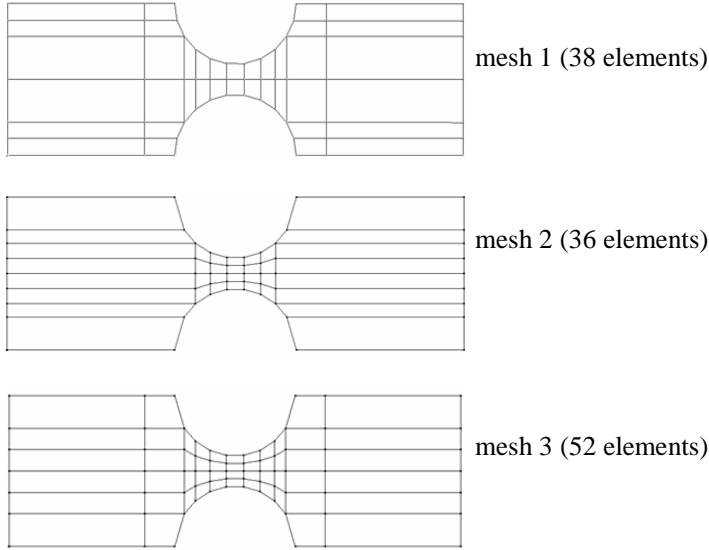mesh 1 (38 elements)

mesh 2 (36 elements)

mesh 3 (52 elements)

Figure 2: Meshes for the notched plate problem.

reference value $K_{tn}$ = 1.141 is taken from

$$K_{tn} = 3.065 - 3.472\frac{2r}{H} + 1.009\left(\frac{2r}{H}\right)^2 + 0.405\left(\frac{2r}{H}\right)^3 \tag{20}$$

given by [Pilkey and Pilkey (2008)] for an infinitely long plate in a state of plane stress.

The contour of $\sigma_{xx}/q$ depicted in Fig. 4 shows that the notches are sufficiently far from the edges $x = 0$ and $x = L$ to make insignificant the influence of longer plates on the calculated $K_t$.

The midsurface distribution of $\sigma_{xx}/\sigma_n$ along the plate width at $x = L/2$ is plotted in Fig. 5a in a suitable scale to highlight the small interelement discontinuity. At this point it should be remembered that the interelement traction continuity is enforced to be satisfied only in a weak sense according to (11). It is also plotted in Fig. 5b the distribution of $\sigma_{xx}/\sigma_n$ along the plate thickness at $(x,y) = (L/2, r)$ or $(L/2, H - r)$, where the maximum value $\sigma_{xx}/\sigma_n = 1.144$ for the whole plate is shown.

Finally, results of $K_t/K_{tn}$ given in Tab. 2 using different values of $r/H$ confirm the good performance of HTS(9,4) element in mesh 2. Although this model has 21501 degrees of freedom, the computing time to solve the linear system was 14 s due to the advantage taken from the 99.42% matrix sparsity. The numerical tests was
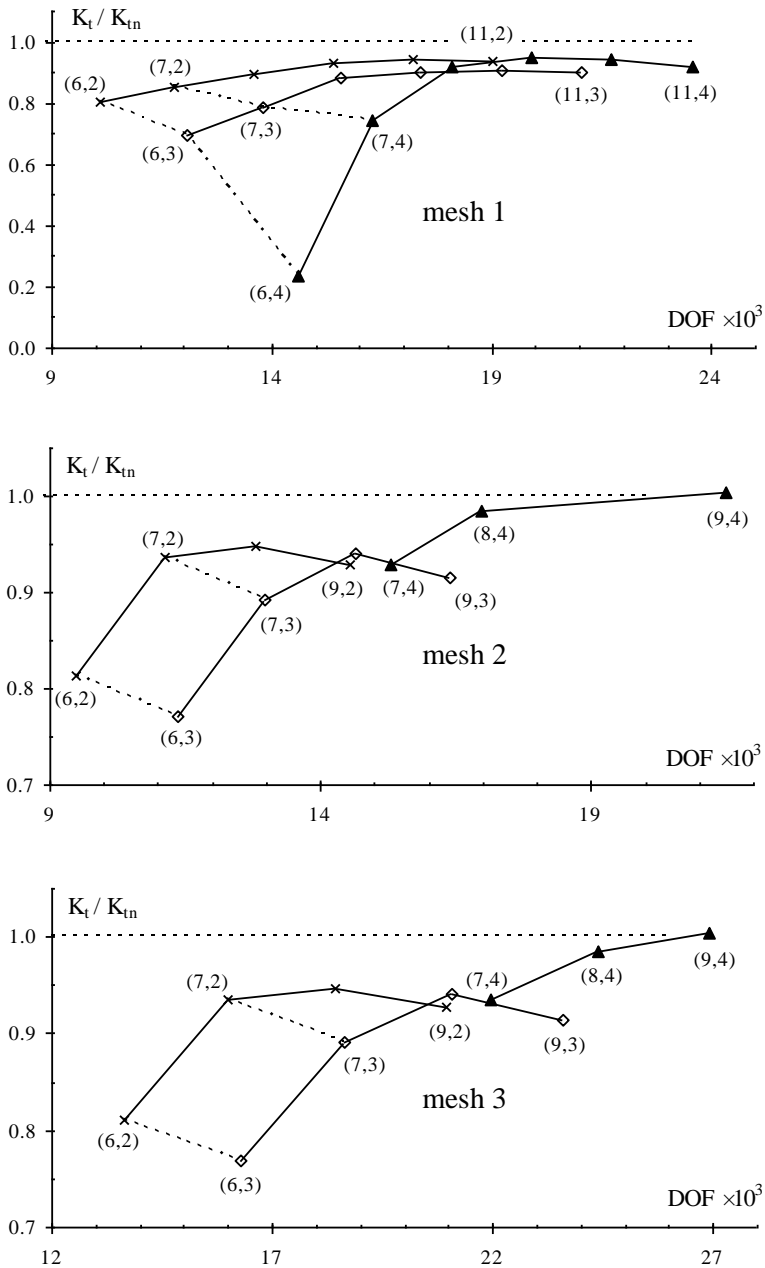
Figure 3: Results of $K_t/K_{tn}$ for r = 0.4 H under p-refinement.

Table 2: Stress concentration factors obtained with mesh 2 under p-refinement

| $r/H$ | $K_{tn}$ (20) | $K_t/K_{tn}$ | | | | | | | | | | | | |
|---|---|---|---|---|---|---|---|---|---|---|---|---|---|---|
| | | (5,2) | (6,2) | (7,2) | (8,2) | (9,2) | (5,3) | (6,3) | (7,3) | (8,3) | (9,3) | (7,4) | (8,4) | (9,4) |
| 0.1 | 2.414 | 0.586 | 0.596 | 0.766 | 0.781 | 0.767 | 0.403 | 0.633 | 0.873 | 0.941 | 0.921 | 0.612 | 1.022 | 0.973 |
| 0.2 | 1.864 | 0.728 | 0.781 | 0.894 | 0.908 | 0.891 | 0.453 | 0.802 | 0.905 | 0.953 | 0.930 | 0.832 | 0.997 | 1.015 |
| 0.3 | 1.433 | 0.903 | 0.877 | 0.944 | 0.990 | 1.038 | 0.488 | 0.836 | 0.926 | 0.998 | 1.018 | 0.899 | 1.031 | 1.053 |
| 0.4 | 1.141 | 0.343 | 0.813 | 0.937 | 0.948 | 0.929 | 0.474 | 0.772 | 0.892 | 0.940 | 0.915 | 0.929 | 0.985 | 1.003 |
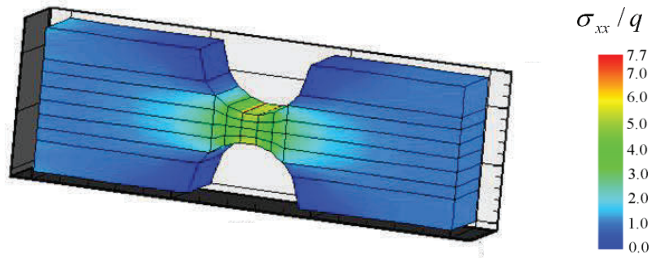
Figure 4: Contour of $\sigma_{xx}/q$ for r/H = 0.4 obtained with mesh 2 of HTS(9,4) elements.
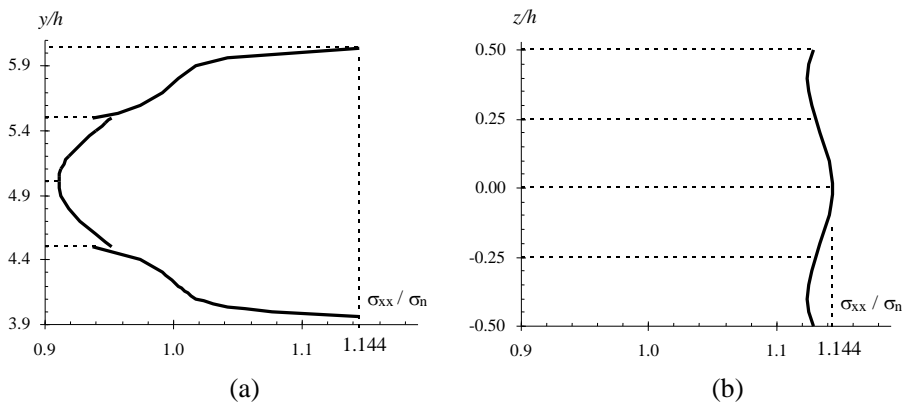


(a)

(b)

Figure 5: Distribution of $\sigma_{xx}/\sigma_n$ for r = 0.4 H obtained with mesh 2 of HTS(9,4) elements: (a) in the midsurface along the plate width at x = L /2; (b) along the plate thickness at (x, y) = (L /2, r) or (L /2, H–r).

carried out in a PC-Computer with Intel Core Duo 2.93 GHz, 8 GB RAM, running Windows XP.

### 3.2 Cracked plate

In the second set of tests, the stress intensity factor $K_I$ is evaluated for the cracked plate depicted in Fig. 6. The notches of Fig. 1 are replaced by one crack of length *a* and the 48-element mesh of Fig. 7 is used in the analysis.

As the plate is in a state of plane stress, the stress intensity factor is evaluated by means of
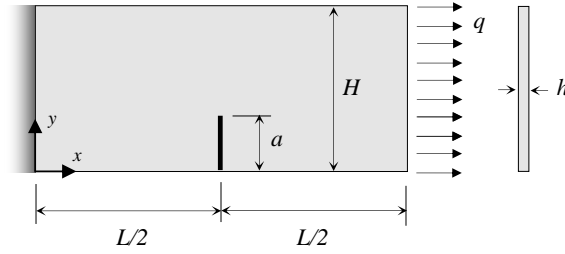
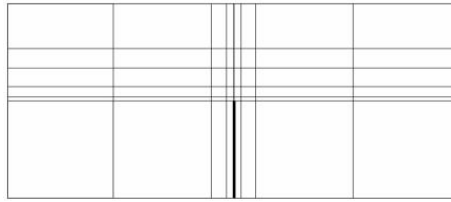$$K_I = \sqrt{EG}. \tag{21}$$

Figure 6: Cracked plate.



Figure 7: 48-element mesh for the cracked plate problem.

The strain energy release rate

$$G = -\frac{1}{h}\frac{\partial U}{\partial a} \tag{22}$$

has the derivative $\partial U/\partial a$ numerically replaced by the ratio between the strain energy change $\Delta U$ and the small value $\Delta a$ assigned to the crack extension. In the present finite element formulation, the strain energy is evaluated from

$$U = \frac{1}{2}\mathbf{X}^{\mathrm{T}}\mathbf{F}\mathbf{X} \tag{23}$$

in which $\mathbf{F}$ refers to the assembled equation that comes from each element contribution (15) and $\mathbf{X}$ results from the equation solution. The stress intensity factors for several crack lengths obtained with 48-element mesh under $p$-refinement are compared in Tab. 3 with

$$K_{ref} = \beta\, q\sqrt{\pi a} \quad \beta = \sqrt{\frac{2H}{\pi a}\tan\frac{\pi a}{2H}}\;\frac{0.752 + 2.02\frac{a}{H} + 0.37\left(1 - \sin\frac{\pi a}{2H}\right)^{3}}{\cos\frac{\pi a}{2H}} \tag{24}$$

found in [Tada, Paris and Irwin (2000)]. Figure 8 shows the contour of $\sigma_{xx}/q$ in a small region around the crack tip for $a/H = 0.5$ obtained with mesh of HTS(6,3) elements. Although this model has 12798 degrees of freedom, it involves a 99.81% sparse matrix.

Table 3: Stress intensity factors obtained with 48-element mesh under p-refinement

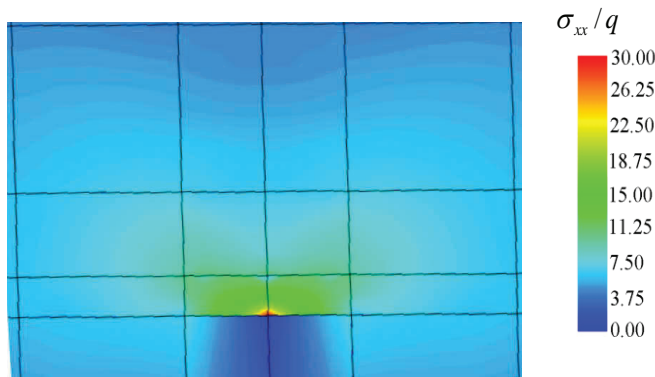| $a/H$ | $K_{ref}$ Eq. (24) | $K_I/K_{ref}$ | | | |
|---|---|---|---|---|---|
| | | (4,2) | (6,3) | (7,3) | (8,4) |
| 0.1 | 2.119 | 1.011 | 0.999 | 0.994 | 0.996 |
| 0.2 | 3.426 | 1.018 | 1.005 | 1.004 | 1.000 |
| 0.3 | 5.081 | 1.022 | 1.006 | 1.002 | 1.005 |
| 0.4 | 7.473 | 1.019 | 1.002 | 0.997 | 1.004 |
| 0.5 | 11.203 | 1.017 | 0.998 | 0.987 | 1.041 |
| 0.6 | 17.554 | 1.020 | 0.996 | 0.994 | 0.943 |
| 0.7 | 29.898 | 1.025 | 0.998 | 0.995 | 0.999 |
| 0.8 | 60.122 | 1.037 | 1.003 | 0.995 | 1.000 |



Figure 8: Contour of $\sigma_{xx}/q$ around the crack tip for a/H = 0.5 obtained with mesh of HTS(6,3) elements.

### 3.3  *Kinked crack plate*

In this third example, the crack of Fig. 6 is replaced by the kinked crack of Fig. 9. The 36-element mesh depicted in Fig. 10 is now used to evaluate the stress intensity factor for a crack length $a = 0.25\sqrt{2}H$ and a kink tip length $t = 0.025\,H$.

The expression (21) is still used to evaluate $K_I$, since the contribution of any crack-opening mode to $G$, rather than mode I, is negligible in this problem as pointed out by [Tracey and Cook (1977)]. Figure 11 shows the results of $K_I/K_{ref}$ under
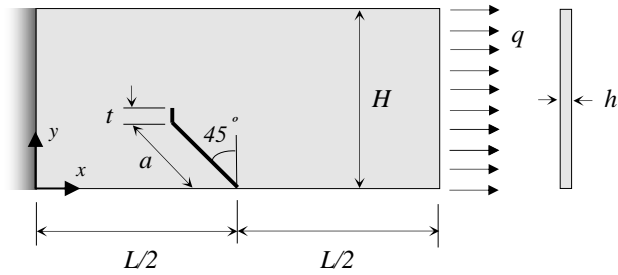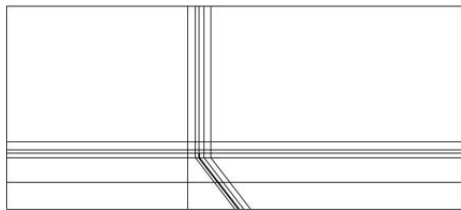
Figure 9: Kinked crack plate.



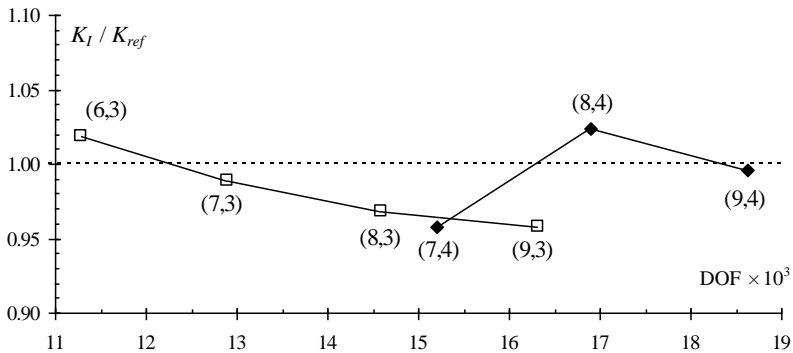Figure 10: 36-element mesh for the kinked crack plate problem



Figure 11: Results of $K_I/K_{ref}$ under p-refinement.

*p*-refinements, where the reference value

$$K_{ref} = 1.52q\sqrt{\frac{1.1\pi}{4}}H = 44.677 \tag{25}$$

is found in [Tracey and Cook (1977)].

The result obtained with mesh of HTS(9,4) elements are compared in Tab. 4 with

results obtained using special crack element models. The HTS(9,4) model has 16893 degrees of freedom, but deals with a 99.65% sparse matrix.

Table 4: Stress intensity factor $K_I$.

| $K_{ref}$ Eq. (25) | Tracey and Cook (1977) | Maiti (1992) | Freitas and Ji (1996b) | HTS (9,4) |
|---|---|---|---|---|
| 44.677 | 42.890 | 44.621 | 44.751 | 44.497 |

## 4   Conclusions

The results show that the hexahedral hybrid-Trefftz elements can handle three-dimensional modeling of thin plates with geometric discontinuities. Good convergence rates under p-refinement are observed even for coarse meshes around the discontinuities. Accurate estimates for stress concentration factors and stress intensity factors are found. Many degrees of freedom are involved, but substantial memory and computing time are saved in the assemblage and problem solution by taking numerical advantage of the high sparsity, that has been greater than 99%.

## References

**Babuška, I.** (1973): The finite element method with Lagrange multipliers. *Numer Math,* vol. 20, no. 3, pp. 179-192.

**Bathe, K. J.** (1996): *Finite element procedures.* Prentice Hall, Englewood Cliffs.

**Brezzi, F.** (1974): On the existence, uniqueness and approximation of saddle point problems arising from Lagrangian multipliers. *RAIRO*, vol. 8, no. 2, pp. 129-151.

**Bussamra, F. L. S.; Lucena Neto, E.; Raimundo Jr., D. S.** (2012): Hybrid quasi-Trefftz 3-D finite elements for laminated composite plates. *Comput Struct,* vol. 92-93, pp. 185-192.

**Bussamra, F. L. S.; Pimenta, P. M.; Freitas, J. A. T.** (2001): Hybrid-Trefftz stress elements for three-dimensional elastoplasticity. *Comput Assist Mech Eng Sci*, vol. 8, pp. 235-246.

**Cook, R. D.; Malkus, D. S.; Plesha, M. E.; Witt R. J.** (2002): *Concepts and applications of finite element analysis.* John Wiley, New York.

**Dong, L.; Atluri, S. N.** (2012a): Development of 3D T-Trefftz Voronoi cell finite elements with/without spherical voids &/or elastic/rigid inclusions for micromechanical modeling of heterogeneous materials. *Comput Mater Contin*, vol. 29, no. 2, pp. 169-211.

**Dong, L.; Atluri, S. N.** (2012b): Development of 3D Trefftz Voronoi cells with ellipsoidal voids &/or elastic/rigid inclusions for micromechanical modeling of heterogeneous materials. *Comput Mater Contin,* vol. 30, no. 1, pp. 39-81.

**Dong, L.; Atluri, S. N.** (2012c): T-Trefftz Voronoi cell finite elements with elastic/rigid inclusions or voids for micromechanical analysis of composite and porous materials. *Comput Model Eng Sci*, vol. 83, no. 2, pp. 183-219.

**Duarte, C. A.; Babuška, I.; Oden, J. T.** (2000): Generalized finite element methods for three-dimensional structural mechanics problems. *Comput Struct*, vol. 77, no. 2, pp. 215-232.

**Freitas, J. A. T.; Bussamra, F. L. S.** (2000): Three-dimensional hybrid-Trefftz stress elements. *Int J Numer Meth Engng*, vol. 47, no. 5, pp. 927-950.

**Freitas, J. A. T.; Cismasiu, C.** (2001): Developments with hybrid-Trefftz stress and displacement elements. *Comput Assist Mech Eng Sci*, vol. 8, pp. 289-311.

**Freitas, J. A. T.; Ji, Z. Y.** (1996a): Hybrid-Trefftz finite element formulation for simulation of singular stress fields. *Int J Numer Meth Engng*, vol. 39, no. 2, pp. 281-308.

**Freitas, J. A. T.; Ji, Z. Y.** (1996b): Hybrid-Trefftz equilibrium model for crack problems. *Int J Numer Meth Engng*, vol. 39, no. 4, pp. 569-584.

**Fu, X. R.; Yuan, M. W.; Cen, S.; Tian, G.** (2012): Characteristic equation solution strategy for deriving fundamental analytical solutions of 3D isotropic elasticity. *Appl Math Mech*, vol. 33, no. 10, pp. 1253-1264.

**Fung, Y. C.; Tong, P.** (2001): *Classical and computational solid mechanics*. World Scientific, Singapore.

**Hinton, E.; Campbell, J. S.** (1974): Local and global smoothing of discontinuous finite element functions using a least squares method. *Int J Numer Meth Engng*, vol. 8, no. 3, pp. 461-480.

**Hinton, E.; Scott F. C.; Ricketts, R. E.** (1975): Local least squares smoothing for parabolic isoparametric elements. *Int J Numer Meth Engng*, vol. 9, no. 1, pp. 235-256.

**Kardestuncer, H.** (1988): *Finite element handbook*. McGraw-Hill, New York.

**Li, Z. C.; Lu, T. T.; Hu, H. Y.** (2004): The collocation Trefftz method for biharmonic equations with crack singularities. *Eng Anal Bound Elem*, vol. 28, no. 1, pp. 79-96.

**Maiti, S. K.** (1992): A finite element for variable order singularities based on the displacement formulation. *Int J Numer Meth Engng*, vol. 33, no. 9, pp. 1955-1974.

**Pian, T. H. H.** (1995): State-of-the-art development of hybrid/mixed finite element

method. *Finite Elem Anal Des*, vol. 21, no. 1-2, pp. 5-20.

**Pian, T. H. H.; Wu, C. C.** (2006): *Hybrid and incompatible finite element methods*. Chapman, Boca Raton.

**Pilkey W. D.; Pilkey, D. F.** (2008): *Peterson's stress concentration factors*. John Wiley, Hoboken.

**Pissanetsky, S.** (1984): *Sparse matrix technology*. Academic Press, London.

**Slaughter, W. S.** (2002): *The linearized theory of elasticity*. Birkhäuser, Boston.

**Souza, C. O.; Proença, S. P. B.** (2011): A hybrid-Trefftz formulation for plane elasticity with selective enrichment of the approximations. *Int J Numer Meth Biomed Engng*, vol. 27, no. 5, pp. 785-804.

**Tada, H.; Paris, P. C.; Irwin, G. R.** (2000): *The stress analysis of cracks handbook*. ASME Press, New York.

**Tracey, D. M. ; Cook, T. S.** (1977): Analysis of power type singularities using finite elements. *Int J Numer Meth Engng*, vol. 11, no. 8, pp. 1225-1233.

**Wang, M. Z.; Xu, B. X.; Zhao, Y. T.** (2012): General representations of polynomial elastic fields. *J Appl Mech*, vol. 79, no. 2, pp. 021017-1 - 021017-8.

**Washizu K** (1982): *Variational methods in elasticity and plasticity*. Pergamon Press, Oxford.

**Williams, M. L.** (1952): Stress singularities resulting from various boundary conditions in angular corners of plates in extension. *J Appl Mech*, vol. 19, pp. 526-528.

**Wunderlich, W.; Pilkey, W. D.** (2002): *Mechanics of structures: variational and computational methods*. CRC Press, Boca Raton.